Main Manuscript for

Trehalose dimycolate inhibits phagosome maturation and promotes intracellular *M. tuberculosis* growth via noncanonical SNARE interaction

Carolina Santamaria[1,2], Kyle J. Biegas[3,4], Christi Y. Kim[2], Jessica Cabral[2], James R. Lee[2], Benjamin M. Swarts[3,4], M. Sloan Siegrist[1,2,*]

[1]Molecular & Cellular Biology Program, University of Massachusetts, Amherst, Massachusetts 01003, USA;
[2]Department of Microbiology, University of Massachusetts, Amherst, Massachusetts 01003, USA;
[3]Department of Chemistry and Biochemistry, Central Michigan University, Mount Pleasant, Michigan 48859, USA
[4]Biochemistry, Cell, and Molecular Biology Graduate Program, Central Michigan University, Mount Pleasant, Michigan 48859, USA

*M. Sloan Siegrist

Email: siegrist@umass.edu

Author Contributions: C.S., B.M.S., and M.S.S. designed research; C.S., K.J.B., C.Y.K., J.C., and J.R.L. performed research; C.S., B.M.S., and M.S.S. analyzed data; and C.S., B.M.S., and M.S.S. wrote the paper.

Competing Interest Statement: M.S.S. is a co-founder and acting CSO of Latde Diagnostics. M.S.S. and C.S. are listed as inventors on U.S. Patent Application No. 63/260,897. Additionally, M.S.S. received research funding through NIH Grant R43 AI186702 in support of Latde Diagnostics.

Classification: Biological Sciences, Microbiology

Keywords: *Mycobacterium tuberculosis*, cell envelope, click chemistry, SNARE, phagosome

This PDF file includes:

Main Text
Figures 1 to 6
Supplementary Materials and Methods
Supplementary Figures

Abstract

Mycobacterial cell envelopes are rich in unusual lipids and glycans that play key roles during infection and vaccination. The most abundant envelope glycolipid is trehalose dimycolate (TDM). TDM compromises the host response to mycobacterial species via multiple mechanisms, including inhibition of phagosome maturation. The molecular mechanism by which TDM inhibits phagosome maturation has been elusive. We find that a clickable, photoaffinity TDM probe phenocopies native TDM in macrophage host cells and binds several host SNARE proteins, including VTI1B, STX8, and VAMP2. VTI1B and STX8 normally promote endosome fusion by forming a complex with VAMP8. However in the presence of native TDM or *Mycobacterium tuberculosis*, VTI1B and STX8 can complex with VAMP2, which in turn inhibits VAMP8 binding. VAMP2 inhibits phagosome maturation and promotes intracellular *M. tuberculosis* replication. Thus one mechanism by which TDM constrains the innate immune response to *M. tuberculosis* is via non-canonical SNARE complexation.

Significance Statement

Glycolipids from the *Mycobacterium tuberculosis* cell envelope, particularly trehalose dimycolate (TDM), play key roles in subverting the immune response to this intracellular pathogen. How subversion occurs is often unclear because glycans and lipids are technically challenging to study in cells. We discovered that a TDM-mimicking chemical probe interacts with three host SNARE proteins, including two that regulate endosome fusion and one that does not. The presence of TDM or *M. tuberculosis* triggers abnormal binding of these SNAREs, which in turn inhibits the fusion of *M. tuberculosis*-containing phagosomes with lysosomes and promotes *M. tuberculosis* replication. Our work provides an unusual example of a bacterial pathogen restricting the immune response via glycolipid-SNARE interactions.

Main Text

Introduction

The cell envelope of mycobacteria shapes the innate immune response to these organisms. Surrounding the cytoplasm, the mycobacterial envelope consists of a peptidoglycan cell wall, an arabinogalactan layer, and a distinctive outer “myco” membrane (Figure 1A) that is unique to the *Corynebacterineae* suborder. The inner and outer leaflets of the mycomembrane are respectively composed of mycolic acids that are covalently attached to arabinogalactan and intercalated glycolipids (1). The most abundant envelope glycolipid, trehalose dimycolate (TDM), has several critical roles in *Mycobacterium tuberculosis* pathogenesis (2). For example, TDM engages several host receptors, including Mincle (Macrophage inducible Ca^{2+}-dependent lectin receptor), to trigger a pro-inflammatory cytokine response and granuloma formation (3–5). TDM can also impair the host response and promote intracellular mycobacterial survival by inhibiting phagosome maturation and acidification in host cell macrophages (6, 7).

During normal phagosome maturation, a microbe-containing phagosome fuses with endosomes and eventually lysosomes. Subsequent acidification of the phagolysosome activates enzymes that destroy the microbe, in turn enabling antigen processing and presentation on the phagocytic cell surface that can initiate adaptive immune responses (8, 9). Inhibition of phagosome maturation is a well-documented strategy for immune evasion across bacterial, protozoan, and fungal species, first observed in *Mycobacterium tuberculosis* and the vaccine *M. bovis* BCG in 1971 (10). In addition to TDM, mycobacterial species use secreted protein effectors and other envelope lipids to inhibit phagosome maturation (11). To date, the reported mechanisms by which TDM or any envelope lipid interferes with normal phagosome maturation are indirect, *e.g.*, inhibition of host signaling pathways (6), and/or speculative, *e.g.*, modulation of phagosome proteome (12–14) and

in vitro inhibition of model liposome fusion (15). Envelope lipids can be released by BCG and the aquatic pathogen *M. marinum* during infection and spread throughout host membranes (16–19). While their physical location in host cells suggests the potential for these lipids to directly interfere with fusion events that are necessary for phagosome maturation, such mechanisms have not been reported in live cells.

One strategy by which other intracellular pathogens hijack phagosome maturation is via host SNAREs (Soluble *N*-ethylmaleimide-Sensitive Factor Attachment Proteins Receptor), membrane-bound mediators of fusion between vesicles and organelles (20, 21). Pathogen interference with the expression and/or function of SNAREs can create a more hospitable intracellular environment by controlling vesicle traffic to and from the phagosome (22, 23). The BCG vaccine alters SNARE recruitment to the phagosome (13, 14, 12), although the downstream consequences on host-BCG interactions have not been demonstrated nor have similar findings yet been reported for pathogenic species such as *M. tuberculosis*. Additionally, while other microbes secrete proteins that mimic or modify the SNAREs, similar-acting mycobacterial proteins have not been identified. Instead, mycobacterial envelope glycolipids like mannose-capped lipoarabinomannan (ManLAM) and its biosynthetic precursor phosphatidylinositol mannoside (PIM) can modulate SNARE recruitment to the phagosome, albeit in ways that are indirect (14) or not yet characterized (12).

Although mycobacterial envelope lipids and glycans influence numerous interactions with the host, significant gaps in mechanistic insight persist due to the technical challenges of tracking and manipulating these components within cells. We focused on TDM, an abundant envelope glycolipid that contributes to the pathophysiology of both tuberculosis infection (2, 24) and BCG vaccination (25) in addition to inhibiting phagosome maturation. Here we synthesize and deploy a clickable, photocrosslinking TDM probe to identify interacting proteins in host cell macrophages. Like native TDM, the probe stimulates a pro-inflammatory cytokine response and interacts with Mincle. Chemical proteomics followed by co-immunoprecipitation experiments revealed that the TDM probe interacts with host SNAREs. Three of the SNAREs that we identified–VTI1B, STX7, and STX8–comprise a late endosome complex that normally binds VAMP7 or VAMP8 to mediate fusion with other endosomes or with lysosomes (20, 26, 27). The fourth SNARE that we identified, VAMP2, can associate with endosomes and lysosomes but it is not known to bind VTI1B, STX7, or STX8 (20, 28, 29). We find that VAMP2 forms a non-canonical complex with VTI1B and STX8 specifically in the presence of native TDM or *M. tuberculosis*. During macrophage infection, VAMP2 inhibits VAMP8 complexation with VTI1B and STX8, inhibits phagosome maturation, and promotes *M. tuberculosis* replication. Thus, TDM drives non-canonical SNARE complexation to benefit intracellular *M. tuberculosis* survival (7, 30–32).

Results

Mycobacterial Glycolipid Probe O-x-AlkTDM Recapitulates TDM Activity and Binding in Macrophages

How TDM inhibits phagosome maturation is unknown. We reasoned that identification of macrophage proteins that interact with TDM could provide clues to the mechanism of TDM's inhibition. However, glycolipid-protein interactions are transient and generally weaker than protein-protein interactions, and therefore less amenable to analysis using traditional biochemical approaches. We previously reported a clickable, photocrosslinking trehalose monomycolate (TMM) probe, which is converted by live mycobacteria into TDM, and used this technology to identify TDM-interacting proteins in the model organism *M. smegmatis* (33). To identify TDM-interacting proteins in host cells, we synthesized O-x-AlkTDM, a direct mimic of TDM bearing an alkyne and a diazirine with linear, truncated lipid chains (Figure 1C). The diazirine enables crosslinking upon ultraviolet light irradiation while the alkyne enables copper-catalyzed alkyne-azide cycloaddition (CuAAC) to attach azide-bearing detection moieties. The structure of O-x-AlkTDM was inspired by the well-established, TDM-mimicking adjuvant trehalose-6,6-dibehenate (TDB), which elicits a macrophage

response like native TDM despite its simplified lipid chains (34). The goal of the compound design was to create a probe that enables covalent capture and pull-down assays while recapitulating the phenotypes of native TDM or TDB adjuvant in host cells (Figure 1B). O-x-AlkTDM was chemically synthesized using our established strategy and its key functionalities were validated in a photocrosslinking experiment with bovine serum albumin (Supporting Information (SI), Figures S1-S4).

We first tested whether the O-x-AlkTDM probe stimulates a pro-inflammatory cytokine response. After incubating immortalized bone marrow-derived macrophages (iBMDMs) (36) from C57BL/6 mice with O-x-AlkTDM, we observed that the probe triggered a cytokine response similar to that of TDB, *i.e.*, dose-dependent TNF-α and IL-6 production (Figures 2A-B). We next tested whether O-x-AlkTDM interacts with Mincle, a known receptor for TDM (3, 4, 6, 5). iBMDMs treated with O-x-AlkTDM were irradiated with UV and subjected to CuAAC with TAMRA Biotin Azide (AzTB; Figure 2C). After affinity enrichment and SDS-PAGE, we detected O-x-AlkTDM-interacting proteins via in-gel fluorescence to visualize TAMRA labeling. Immunoblotting then revealed time-dependent interactions between O-x-AlkTDM and Mincle, which peaked at 3 hours (Figure 2D). These findings demonstrate that the O-x-AlkTDM probe elicits a physiologically-relevant innate immune response and can report a known host protein interaction.

Macrophage SNAREs Interact with O-x-AlkTDM

We next investigated whether O-x-AlkTDM could reveal new interactions with host proteins. To prepare samples for chemical proteomics, we again treated iBMDMs with the probe, UV-irradiated, clicked with AzTB, and affinity-enriched prior to LC-MS/MS. Over-Representation Analysis (ORA; (37)) showed significant enrichment of four SNARE proteins in the presence of O-x-AlkTDM: Syntaxin 8 (STX8), Syntaxin 7 (STX7), Vesicle Associated Membrane Protein 2 (VAMP2), and Vesicle Transport through Interaction with t-SNAREs 1B (VTI1B) (Figure 3A). STRING network analysis (38) revealed functional associations between them (Figures 3A-B): STX8, STX7, and VTI1B are part of an endosome complex that can bind to either VAMP7 or VAMP8 to mediate homotypic fusion with other endosomes or heterotypic fusion with lysosomes (26, 27). STX8 has also previously been shown to reside on both latex bead- and BCG-containing phagosomes (14). VAMP2 has primarily been implicated in vesicle exocytosis and in complexes with SNAP25 and STX1A (39); it has not previously been linked to STX8, STX7, or VTI1B (26–29, 40). Co-immunoprecipitation experiments confirmed interactions between O-x-AlkTDM and STX8, VTI1B, and VAMP2 in both iBMDMs and the human cell line THP-1 (Figures 4A-B; we were unable to detect STX7 even from protein lysates).

As expected, most O-x-AlkTDM-SNARE interactions were promoted by UV. However, VAMP2 detection after O-x-AlkTDM affinity purification was consistently independent of UV, in both iBMDMs and THP-1s, despite the UV dependence for the reciprocal experiment (O-x-AlkTDM detection after VAMP2 immunoprecipitation; Figure 4C). While we do not yet understand why O-x-AlkTDM-VAMP2 is detectable without cross-linking, we hypothesize that this interaction is more stable than O-x-AlkTDM-STX8 or O-x-AlkTDM-VTI1B. We frequently observed multiple bands in pulldowns from the O-x-AlkTDM-treated samples, particularly for VTI1B and STX8 (SI, Figure S5). While not definitive, these data suggest that more than one molecule of O-x-AlkTDM may be able to bind to these proteins. Taken together, our data indicate that O-x-AlkTDM interacts with host SNARE proteins STX8, VTI1B, and VAMP2.

Specificity of Glycolipid-SNARE Interactions

Structural variability in glycan head group and/or mycolic acids can modulate the host cell response to TDM (4, 41–43). Therefore, we sought to understand the specificity of O-x-AlkTDM-SNARE interactions. To investigate the role of glycolipid structure, we incubated iBMDMs with two additional probes: O-x-AlkTMM (33), which retains the trehalose sugar and one lipid chain, and x-

AlkFA, which contains a single lipid chain and lacks the trehalose head group (Figure 1C). Like TDM, TMM is a natural constituent of the mycobacterial cell envelope and a reported ligand for Mincle (5, 43). Following UV irradiation, CuAAC with AzTB, and affinity purification, we found that all three probes produced UV- and click-dependent bands. However, x-AlkFA failed to pull down STX8 or VTI1B. While O-x-AlkTMM pulled down both proteins, it did so less efficiently than O-x-AlkTDM (Figure 4D). These findings suggest that glycolipid-SNARE interactions require a glycan head group and are enhanced by the presence of two lipid chains.

To investigate glycolipid-SNARE specificity on the protein side of the interaction, we immunoblotted samples that had been immunoprecipitated for O-x-AlkTDM/TMM-interacting proteins with antibodies to other SNAREs. The repertoire of SNAREs that O-x-AlkTDM/TMM could pull down extended beyond the ones that we identified by proteomics, and included VAMP8, STX6, and STX18 (Figure 4E). VAMP8 mediates endosomal fusion, in complex with VTI1B, STX7, and STX8 (26, 27). As with VAMP2, the O-x-AlkTDM interaction with VAMP8 was not dependent on cross-linking, suggesting that it may be more stable than O-x-AlkTDM-STX6 or O-x-AlkTDM-STX18. STX6 and STX18 are respectively involved in trans-Golgi-endosome and ER-Golgi trafficking (21, 20). STX6 is present on latex bead-containing phagosomes but excluded from BCG-containing phagosomes via an indirect mechanism that depends on the mycobacterial glycolipid mannose-capped lipoarabinomannan (ManLAM) (14). Not all the proteins that we tested pulled down with O-x-AlkTDM; we did not detect interactions between the probe and STX5, a SNARE that mediates trafficking from phagosomes to the trans-Golgi network, nor to GAPDH, a cytosolic enzyme (20, 44) (Figures 4D and SI, Figure S6). We conclude that O-x-AlkTDM selectively interacts with a subset of SNAREs.

Mycobacterium tuberculosis TDM Induces Non-Canonical, VAMP2-containing SNARE Complexation in Macrophages

SNARE complexation pulls membranes together, facilitating fusion necessary for processes like phagosome maturation. SNAREs generally interact to form a stable, four-helix bundle, with Qa-, Qb-, and Qc-SNAREs on one membrane and R-SNAREs on the other membrane (20). SNAREs can sometimes substitute for one another, a property exploited by various intracellular pathogens that disrupt normal complexation via SNARE deubiquitination (45–47) and secreting SNARE-mimicking proteins (48–50). STX7 (Qa-SNARE), VTI1B (Qb-SNARE), and STX8 (Qc-SNARE) on endosomal membranes fuse with VAMP7 or VAMP8 (R-SNAREs) on endosomal and lysosomal membranes *in vitro* (26, 27). VAMP2 is an R-SNARE that can also associate with endosomes and lysosomes but is not known to interact with STX7, VTI1B, or STX8 (20, 26).

We wondered whether TDM-SNARE interactions might induce and/or mark the formation of non-canonical complexes in which VAMP2 substitutes for VAMP8. We first asked whether VAMP2-containing complexes were detectable in the presence of *M. tuberculosis* by immunoprecipitating SNAREs from iBMDMs infected with *M. tuberculosis* $mc^2$6206. We found that VTI1B and STX8 interact with each other regardless of infection status (Figure 5A). By contrast, VTI1B and STX8 partner with VAMP2 only in the presence of *M. tuberculosis* and with a concomitant reduction in binding to VAMP8 (Figure 5A). Protein levels of VAMP2, VAMP8, VTI1B, and STX8 in iBMDMs were similar with or without the pathogen (Figure 5B), suggesting a difference in protein interactions rather than expression.

To test whether TDM was sufficient for non-canonical SNARE complexation, we incubated iBMDMs with latex beads coated with IgG, O-x-AlkTDM, or native TDM. While VTI1B and STX8 interacted with each other regardless of bead coating, VTI1B and STX8 interacted with VAMP2 only when beads were coated with native TDM (Figure 5C). Thus, despite the ability of the O-x-AlkTDM probe to interact with VTI1B, STX8, and VAMP2 (Figure 4), native TDM structure is required for detectable complexation of these proteins. Unlike *M. tuberculosis* infection, TDM-bead incubation did not alter VAMP8 complexation with VTI1B and STX8 (Figure 5C). This discrepancy may reflect differential

abundance and/or presentation of TDM, *i.e*., bead vs. surface of bacterium, and/or may indicate that additional *M. tuberculosis* factors are necessary to inhibit normal SNARE complexation.

To test whether non-canonical SNARE complexation triggered by *M. tuberculosis* was dependent on VAMP2, we compared wild-type to *VAMP2* knockout THP-1 cells. As in iBMDMs, we observed that VTI1B and STX8 interact with VAMP2 only in infected THP-1s, with concomitant reduction in VAMP8 complexation. However, in *VAMP2* knockout THP-1s, VAMP8 interactions with VTI1B and STX8 were similar in the presence or absence of *M. tuberculosis* (Figures 6A-B and SI, Figure S8). Taken together, our data suggest that *M. tuberculosis* TDM triggers the formation of non-canonical, VAMP2-containing SNARE complexes at the expense of cognate VAMP8-containing complexes.
To assess the spatial distribution of VAMP2, we nucleofected iBMDMs with a previously-described plasmid expressing eGFP-VAMP2 (51) (SI, Figure S7). While eGFP-VAMP2 localized near intracellular *M. tuberculosis*, as expected, its subcellular distribution did not obviously change in infected vs. uninfected iBMDMs (Figure 6C). These data suggest that either *M. tuberculosis* changes the behavior of VAMP2 that is already in the vicinity of the pathogen, or that only a small pool of VAMP2, not detectable with our current methods, is recruited to *M. tuberculosis*-containing phagosomes.

VAMP2 Promotes *M. tuberculosis* Survival in Macrophages

In unactivated macrophages, *M. tuberculosis* can replicate well in part because it delays the fusion of phagosomes with low-pH lysosomes (10, 52–54). Given that VTI1B, STX8, and VAMP8 mediate endosome fusion, and that VAMP8 polymorphisms are associated with human susceptibility to tuberculosis (55), we hypothesized that VAMP2-dependent disruption of normal VTI1B-STX8-VAMP8 complexation inhibits phagosome-lysosome fusion and promotes *M. tuberculosis* replication. To test, we first infected THP-1s with mEmerald-expressing *M. tuberculosis* and quantified the proportion of bacteria that were spatially coincident with LysoTracker, a dye that stains acidic compartments. Approximately three- to four-fold more *M. tuberculosis* were spatially coincident with LysoTracker in *VAMP2* knockout compared to wild-type THP1-s (Figure 6D), suggesting that VAMP2 contributes to the ability of *M. tuberculosis* to inhibit phagosome-lysosome fusion.

To investigate a role for VAMP2 in *M. tuberculosis* replication, we then infected wild-type and eGFP-VAMP2-expressing iBMDMs (which express both eGFP-VAMP2 (51) and VAMP2, the latter to higher levels than wild-type; SI, Figure S7) and wild-type and *VAMP2* knockout THP-1s and plated for colony-forming units at various time points. We found that *M. tuberculosis* replicated significantly better in eGFP-VAMP2-expressing iBMDMs compared to wild-type, and more poorly in *VAMP2* knockout THP-1s compared to wild-type (Figures 6E-F). These findings indicate that VAMP2 promotes *M. tuberculosis* replication in addition to inhibiting phagosome acidification.

Discussion

Lipids and glycans are released from the mycobacterial envelope during infection and affect host cell function. Chief among these bioactive molecules is TDM, a highly abundant envelope glycolipid that induces granuloma formation, stimulates pro-inflammatory cytokine production, and inhibits phagosome maturation (2, 3, 7, 15, 30). Despite the importance of TDM and other envelope components to *M. tuberculosis* infection and *M. bovis* BCG vaccination, the mechanistic details of how TDM subverts the immune response have remained unclear. To facilitate the study of TDM in host cells, we drew on recent advances in chemical techniques to profile glycan- and lipid-protein interactions (33, 56–58). We found that the photocrosslinking, clickable TDM probe O-x-AlkTDM recapitulates the effects of TDM on macrophages and interacts with host SNAREs previously implicated in endosome fusion, including VTI1B, STX8, and potentially STX7. We also discovered that a different O-x-AlkTDM-interacting SNARE, VAMP2, forms a non-canonical complex with VTI1B and STX8 in the presence of native TDM or *M. tuberculosis*, with a reduction in VAMP8

complexation in the latter condition. Many other intracellular pathogens usurp SNARE function; they do so by secreted protein effectors that mimic, degrade, or modify the SNAREs (23, 48–50, 22). To our knowledge, this is the first report of a bacterial lipid or glycan interfering with SNARE function.

How does TDM promote VAMP2 interaction with STX8 and VTI1B? O-x-AlkTDM directly interacts with several SNAREs, all of which are predicted to have transmembrane domains. As mycobacterial envelope lipids, including TDM, can traffic throughout the endocytic network (16–19), we hypothesize that TDM inhibits phagosome maturation by intercalating into host membranes and interacting with SNARE transmembrane domains (Figure 6G). Further application of O-x-AlkTDM may enable precise identification of these binding sites, *e.g.*, by quantitative crosslinking mass spectrometry. Given that O-x-AlkTDM can interact with VTI1B, STX8, and VAMP2 (Figure 4), but seemingly does not trigger non-canonical complexation of these SNAREs like TDM (Figure 5C), future iterations of glycolipid probes with more-native like lipid chain structures are high-priority targets for development (59, 60).

Model and mammalian cell membranes rigidify in the presence of TDM (61, 62). Many SNAREs localize to ordered membrane regions (63) or, like VAMP2, undergo structural changes that promote complexation (64). The transmembrane domain of VAMP2 in particular is sensitive to lipid bilayer composition (65). More broadly, membrane lipids are well-known to affect SNARE clustering, conformation, and fusion (66, 67). Thus, we posit that TDM-triggered changes to the biophysical milieux of host membranes promote complexation of R-SNARE VAMP2 with Q-SNAREs VTI1B, STX8, and STX7 (Figure 6G). In this model, VAMP2 engagement inhibits complexation of the Q-SNAREs with cognate R-SNARE VAMP8. While TDM could promote non-canonical complexation via its interactions with VTI1B, STX8, and/or VAMP2, we favor the latter because VAMP2 is known to be impacted by lipid composition (64, 65) and because O-x-AlkTDM interacts especially tightly with VAMP2 compared to VTI1B or STX8 (Figure 4B).

While VTI1B, STX8, and STX7 likely reside on the *M. tuberculosis*-containing phagosome, the nature of the R-SNARE target membranes is not yet clear. For example, VAMP2 and VAMP8 may both reside on lysosomal membranes (Figure 6G). In this scenario, TDM-triggered engagement of VTI1B, STX8, and STX7 with VAMP2 results in a non-functional complex and stalling of phagosome-lysosome fusion. Alternatively, or additionally, VAMP2 may reside on the membrane of a different vesicle and inhibit the fusion of VAMP8 lysosomes with VTI1B/STX8/STX7-containing phagosomes. High resolution imaging in macrophages, enabled by the clickable tag on O-x-AlkTDM, together with *in vitro* systems with purified organelles, may provide spatial and topological insights into how TDM disrupts vesicle trafficking.

VAMP2 was previously identified as a constituent of the macrophage phagosome proteome that promotes phagocytosis of *Escherichia coli* (68). While we do observe a contribution of VAMP2 to *M. tuberculosis* uptake, the kinetics of replication indicate that VAMP2 additionally promotes intracellular *M. tuberculosis* growth (Figure 6E-F), likely via its effect on phagosome maturation (Figure 6D). Most studies on VAMP2 have focused on its role in secretory vesicles and neuronal exocytosis, raising the possibility that TDM interaction with this SNARE could affect exocytosis from *M. tuberculosis*-infected macrophages, an additional pathway for immune modulation (69). This is especially intriguing given that mycobacterial glycolipids, including TDM, eventually traffic to lysosome-like compartments that are exocytosed (16, 70).

The BCG vaccine does not reliably protect against adult pulmonary tuberculosis, the most common form of the disease. Many groups have developed new recombinant strains, methods of preparation, and modes of administration to enhance the vaccine's efficacy. BCG, like *M. tuberculosis*, inhibits phagosome maturation (10), which in turn decreases antigen processing, the Th1 response, and efficacy (71–74). Targeting of the TDM-VAMP2 interaction has the potential to

enhance antigen presentation and other aspects of *in vivo* immunogenicity for live, attenuated vaccines such as BCG.

Materials and Methods

Strains and media

We used *M. tuberculosis* mc^{2}6206 (H37Rv Δ*panCD* Δ*leuCD* (75)), in some cases transformed with pMV261-mEmerald for imaging (provided by Drs. Chris Sassetti and Christina Baer, University of Massachusetts Medical School). *M. tuberculosis* strains were cultured using Middlebrook 7H9 (liquid) or 7H10 (agar) supplemented with 10% Middlebrook Oleic Albumin Dextrose Catalase (OADC), 0.5% glycerol, 0.05% Tween 80, and kanamycin (20 µg/ml) or hygromycin (50 µg/ml) when necessary. Because *M. tuberculosis* mc^{2}6206 is a double auxotroph, media were additionally supplemented with 50 µg/ml l-leucine (Sigma) and 24 µg/ml pantothenic acid (Sigma).

Human monocyte/macrophage cell line THP-1 and immortalized bone marrow derived macrophages (iBMDM) from C57BL/6J mice were respectively gifts of Drs. Barbara Osbourne, University of Massachusetts Amherst, and Christopher Sassetti, University of Massachusetts Medical School (36). *VAMP2* knockout and wild-type THP-1 cells were purchased from Ubigene Biosciences, Guangzhou Science City, Guangdong, China (Cat # YKO-H1108). THP-1s were maintained in suspension in RPMI 1640 medium (Genesee Scientific) supplemented with 10% (v/v) heat-inactivated fetal bovine serum (FBS; Fisher Scientific), antibiotic-antimycotic (1% containing penicillin G, streptomycin, and amphotericin B), 1 mM sodium pyruvate, and 10 mM HEPES (all from Genesee Scientific) and maintained in a humidified incubator at 37 °C with 5% CO_2 in air. iBMDMs were maintained in Dulbecco's Modified Eagle Medium (DMEM; Genesee Scientific) supplemented with 10% FBS, 2 mM l-glutamine, and 10 mM HEPES and maintained in a humidified incubator at 37 °C with 5% CO_2 in air. THP-1s were differentiated into macrophages by incubating cells with 200 nM, phorbol-12-myristate 13-acetate (PMA; Sigma) for 48 hr.

Protein photocrosslinking and analysis

Stock solutions of synthetic O-x-AlkTDM, O-x-AlkTMM, and O-x-Alk-fatty acid (Figure 1C) were prepared in anhydrous DMSO at concentrations of 100 mM and stored at - 20 °C. Other reagent stocks used in typical copper-catalyzed alkyne-azide cycloaddition (CuAAc) reactions included sodium ascorbate (60 mM in H_2O, always freshly prepared); TBTA ligand (Click Chemistry Tools; 6.4 mM in DMSO; stored at –20 °C); $CuSO_4$ (50 mM in H_2O, stored at room temperature (RT)); TAMRA biotin azide (AzTB, Click Chemistry Tools, 10 mM in DMSO, stored at -20 °C). Probes were diluted to 100 µM in DMSO or DMEM and added directly to the cells in solution or used to coat 100-mm cell culture dishes. Coated dishes were dried in a biosafety cabinet overnight. $5x10^6$ iBMDMs or differentiated THP-1s/plate were seeded onto the coated dishes and incubated for indicated time. Alternatively, macrophages were incubated +/- probe in solution for indicated period. Probe-treated and untreated control macrophages were then UV-irradiated (15-watt, 365 nm UV lamp) for 10 min on ice. Cells were washed with cold PBS and lysed with Pierce RIPA buffer (1 mM PMSF, 1x complete EDTA free protease inhibitor; Thermo Fisher). To reduce capture of endogenous biotinylated proteins, 500 µl of protein lysate was pre-cleaned using 50 µl of Pierce NeutrAvidin Agarose (Thermo Fisher) that was initially washed twice with phosphate-buffered saline (PBS) and twice with RIPA lysis buffer. Beads and lysates were incubated overnight with constant rotation at 4 ºC. Beads were then centrifuged at 3000 x g for 3 min and the protein concentrations of the supernatants were quantitated using Pierce bicinchoninic acid (BCA) assay (Thermo Fisher). Prior to CuAAc, protein concentrations were normalized using RIPA buffer. Lysates were clicked with AzTB for 2 hr with constant shaking at 37 ºC using the following typical CuAAC reaction on 187.5 µl of lysate with indicated final concentrations: 1 mM copper(II) sulfate (4 µl), 100 µM TBTA (3.12 µl), 1 mM sodium ascorbate (3.4 µl), and 100 µM AzTB (2 µl) to give a final volume of 200 µl. Proteins were precipitated using chloroform/methanol (1:1 v/v) at 4 ºC to

remove excess fluorophore and lipids. Precipitated protein pellets were resuspended in 200 µl of RIPA lysis buffer and incubated at 37 ºC for 10 min for protein solubilization. 15 µl of each sample was saved as pre-enrichment click input. The remaining 185 µl of clicked lysate was incubated with 50 µl of Neutravidin beads that were pre-washed as described above. Beads were washed five times with RIPA buffer (200 µl) and five times with PBS (200 µl) via a series of centrifugation steps at 3000 x g for 3 min. Biotinylated proteins were eluted by adding 30 µl of 4x Laemmli loading sample buffer (BioRad) and boiled at 95 ºC for 15 min. ~10-15 µg of input sample (click lysates) and eluted proteins were resolved by SDS-PAGE and analyzed by in-gel fluorescence. The rhodamine channel was used to detect TAMRA-labeled proteins and Coomassie staining was used to detect total protein (Cytiva; Amersham ImageQuant™ 800 Western blot imaging system).

For immunoblotting, 10 µg of the input controls and 15 µL of eluted proteins were resolved by 12% SDS-PAGE. After gel electrophoresis, the proteins were semi-dry transferred onto an Immuno-Blot PVDF membrane (Thermo Fisher). PVDF membrane and filter paper were incubated in a transfer buffer (25 mM Tris, 193 mM glycine, and 20% methanol) and put into a transfer cassette for transfer using the TransBlot Turbo Transfer System. The time of protein transfer was based on protein size, ~7-30 min, for smaller and larger proteins, respectively (25 V). After transfer, the membrane was blocked for 1 hr at room temperature in 5% dry nonfat milk in Tris-buffered saline containing Tween 20, pH 7.4 (50 mM Tris, 0.5 M NaCl, 0.01% Tween 20 (TBST)). Antibodies for immunoblotting were diluted 1:1000 in TBST containing 5% milk. Primary antibodies included: rabbit polyclonal anti-Syntaxin 8 (1:1000), rabbit polyclonal antiserum for VTI1B (1:1000), and mouse monoclonal anti-Synaptobrevin2/VAMP2 (1:1000) from Synaptic Systems, Germany. Mouse monoclonal anti-Mincle (1:1000) from MBL International Corporation, rabbit polyclonal antiserum for Endobrevin/VAMP8 (1:1000 in 5% Bovine Serum Albumin (BSA) in TBST; Synaptic Systems), rabbit polyclonal anti-Syntaxin 5 (1:1000; Cell Signaling), rabbit monoclonal anti-Syntaxin 6 (1:1000; Cell Signaling), rabbit polyclonal anti-Syntaxin 18 (1:1000; Proteintech), rabbit monoclonal anti-GAPDH (1:1000) from Cell Signaling. Anti-rabbit IgG and anti-mouse IgG Horseradish peroxidase (HRP)-linked antibody (1:1000; Cell Signaling). The PVDF membrane was incubated overnight at 4 ºC with constant shaking with primary antibodies. The membrane was then washed with 1x TBST thrice for 10 min. Secondary antibodies (anti-mouse IgG, and anti-rabbit IgG from Cell Signaling) were diluted 1:1000 in TBST containing 5% milk and the membrane was incubated for 1 hr at room temperature with constant shaking. PVDF membrane was then washed thrice with 1x TBST for 10 min and viewed with the Amersham ImageQuant™ 800.

LC–MS/MS analysis

10 µL of samples were run into a BioRad Criterion TGX Precast Gel for ~20 min at 50 V constant so that the samples just entered the stacking gel and did not resolve. Electrophoresis was then stopped, and the gel was stained using Coomassie Blue. The resulting protein bands were excised from the gel and subjected to in-gel tryptic digestion according to Trypsin gold manufacturing protocol (Promega) with modifications. Gel bands were destained with several incubations with 100 mM of ammonium bicarbonate (AB) and 1:1 (v/v) 50 mM ammonium bicarbonate/50% acetonitrile (ACN). Briefly, gel bands were dehydrated using 100% ACN and incubated with 10 mM dithiothreitol in 100 mM AB at 50 °C for 30 min, dehydrated again, and incubated in the dark with 55 mM iodoacetamide in 100 mM AB for 20 min. Gel bands were then washed with AB and dehydrated again. Trypsin gold was prepared to 20 µg/µL in 40 mM AB/10% ACN and added to each gel band so that the gel was completely submerged. Bands were then incubated at 37 °C overnight. Peptides were extracted from the gel by sequential 5-minute incubations with 1 % formic acid/2% ACN, 1:1 (v/v) ACN/water and 1% formic acid in ACN. Pooled supernatants were vacuum-dried and resuspended in 0.1% formic acid for ZipTip cleanup (C_{18} column; Sigma). Samples were then sent to the University of Massachusetts Amherst Mass Spectrometry Core where LC-MS analysis was performed using an Easy-nLC 1000 nanoLC chromatography system interfaced to an Orbitrap Fusion mass spectrometer (Thermo Scientific). Samples were pre-concentrated and desalted on a C18 trap column prior to separation over a 90-min gradient from 0% to 40% mobile

phase B (A:0.1% formic acid in water, B:0.1% formic acid in ACN) at 300 nl/min flow rate with a 75 µm x 15 cm PepMap RLSC column (Thermo Scientific). Mass spectrometry parameters were as follows: ion spray voltage 2000V, survey scan MS1 120k resolution with a 2 s cycle time, interleaved with data-dependent ion trap MS/MS of highest intensity ions with HCD at 30% normalized collision energy. Raw files were analyzed in Proteome Discoverer 2.4 (Thermo Scientific) using the SEQUEST search algorithm using the *Mus musculus* Proteome database. The search parameters used were as follows: 10 ppm precursor ion tolerance and 0.4 Da fragment ion tolerance; up to two missed cleavages were allowed; dynamic modifications of methionine oxidation and N-terminal acetylation. Peptide matches were filtered to a protein false discovery rate of 5% using the Percolator algorithm. Resulting list of proteins were filtered for proteins that had at least 10% coverage and present in three out of the four biological replicates. Only proteins present in the O-x-AlkTDM-treated conditions and not in the controls were considered hits.

Cytokine production

iBMDMs were incubated with indicated concentrations of O-x-AlkTDM or trehalose-6,6-dibehenate (TDB; InvivoGen) for 6 hr. Supernatants were collected at 6 hr and TNF-α and IL-6 production were measured by enzyme-linked immunosorbent assay (R&D Systems, DuoSet ELISA).

Coating green fluorescent latex beads with TDM

200 µl of non-functionalized green fluorescent latex beads (1 µm, Bangs Laboratories) were washed thrice with 1 ml of PBS. Beads were resuspended in 1 ml of 0.1 M borate buffer (Polysciences) and 100 µg Immunoglobulin G (IgG; Sigma), O-x-AlkTDM, or native TDM (Invivogen) were then added. The mixture was incubated overnight at RT with constant rotation. The beads were centrifuged for 10 min and resuspended in 1 ml of 10 mg/ml fat-free BSA (Sigma) in 0.1 M borate buffer and incubated for 1 hr constant rotation. They were then centrifuged for 10 minutes, and the supernatant was discarded. The beads were washed thrice with PBS, then stored in 500 µl of PBS at 4°C in the dark until experimental use.

Immunoprecipitations

Immunoprecipitation from M. tuberculosis-infected macrophages

iBMDMs were infected with *M. tuberculosis* $mc^2$6206 at a multiplicity of infection (MOI) of 1:50 macrophages:bacteria for 4 hr. After 4 hr, cells were washed thrice with l-leucine and pantothenate-supplemented DMEM and incubated an additional 6 hrs in the same medium. Macrophages were then lysed with RIPA buffer. Lysates were filtered twice through 0.2 µm filters (Corning Costar Spin-X; Sigma) and then pre-cleaned with protein G beads (Thermo Fisher) to remove non-specific binding. Protein concentration was quantified by BCA assay and 200 µg of protein was incubated with 2 µg/ml of primary antibody or with isotype control (rabbit IgG or mouse IgG isotype controls; Cell Signaling). Protein-antibody complexes were incubated overnight with constant rotation at 4 ºC. Protein G beads (50 µl) were added to the protein-antibody complexes and incubated for 4 hr with constant rotation at 4 ºC. Beads were washed four times with RIPA buffer and 30 µl of 4x Laemmli loading sample buffer was added to the beads. Beads were boiled for 15 minutes at 95 ºC, and supernatants were collected for immunoblotting. Immunoblotting was performed as described above in "**Protein photocrosslinking and analysis**" using anti-SNARE antibodies and Tidyblot (1:1000; BioRad) in 5% nonfat milk in TBST. Tidyblot was used as a secondary antibody to prevent detection of denatured antibodies.

Immunoprecipitation from bead-incubated macrophages

iBMDMs were incubated with IgG-, O-x-AlkTDM-, or TDM-coated beads at a multiplicity of infection (MOI) of 1:50 macrophages:beads for 1 hr. Cells were then washed thrice with cold PBS and lysed

with RIPA buffer. Lysates were prepared and immunoprecipitations carried out as described in "*Immunoprecipitation from M. tuberculosis-infected macrophages".*

Immunoprecipitation of TDM-SNAREs

As described in "Protein photocrosslinking and analysis", iBMDMs were incubated with O-x-AlkTDM, UV-irradiated, lysed, and subjected to CuAAC with AzTB. Clicked lysates were then chloroform/methanol precipitated and resuspended pellets were immunoprecipitated with antibodies to VAMP2, VTI1B and STX8 at 2 µg/ml. To test for O-x-AlkTDM presence we used in-gel fluorescence (to detect TAMRA) and/or immunoblotted with anti-biotin antibodies (1:1000; 5% nonfat Milk in TBST; Abcam).

eGFP-VAMP2 expression in iBMDMs

Lonza nucleofector with SG Cell Line 4D-Nucleofector™ X Kit S was used to generate eGFP-VAMP2-expressing macrophages. $2x10^5$ iBMDMs were washed and resuspended in the appropriate electroporation buffer. iBMDM cell suspensions were mixed with 2 µg of pEGFP VAMP2 (mouse; Addgene plasmid # 42308 (51). Cells were electroporated using the program FF-100 and immediately transferred to pre-warmed DMEM. Cells were plated in a 24-well plate for recovery, and after 48 hours, were sorted for eGFP-positive cells using BD FACSAria Fusion. Appropriate selection antibiotic was added after 24 hrs of sorting. After 6 days of antibiotic selection, cells were ready for experimental usage. Lysates were immunoblotted using anti-GFP (1:1000 in 5% non-fat milk in 1xTBST; Proteintech) and anti-VAMP2 to test for eGFP-VAMP2 expression (SI, Figure S7). We detected the fusion protein in iBMDMs that were successfully nucleofected with the plasmid, and additionally observed that VAMP2 alone is more abundant in these cells.

Macrophage infections

M. tuberculosis replication

1 ml stock of *M. tuberculosis* mc^26206 (previously frozen at OD ~ 1.0) was thawed and diluted 1:10 in 7H9 medium and incubated at 37 ºC with shaking at 150 rpm for 2-3 days, until the optical density at 600 nm (OD_{600}) reached 0.3. One day prior to infection, iBMDMs were plated in a 96-well plate at a density of 2×10^4 cells per well. THP-1 cells were plated at a density of 4×10^4 cells and differentiated 48 hr before infection. On the day of infection, the bacterial culture was washed twice with PBS, and the OD_{600} was measured. The total *M. tuberculosis* required for the desired MOI was calculated based on this OD_{600} reading and was transferred to DMEM or RPMI 1640 (depending on cell type) supplemented with 50 µg/ml l-leucine and 24 µg/ml pantothenic acid (without antibiotics). Medium was removed from the iBMDM or THP-1 plates, and fresh medium with resuspended *M. tuberculosis* was added at an MOI of 1:10 (macrophages:bacteria), with 200 µl per well. Cells were incubated at 37 ºC with 5% CO_2 for 4 hours. Afterward, the cells were washed thrice with medium, and fresh complete DMEM or RPMI 1640 was added to maintain continuous culture at 37 ºC with 5% CO_2. For colony-forming unit (CFU) plating at 0, 24, 72 hr, and 120 hrs post-infection, macrophages were lysed with 0.1% Triton X-100 for 5 min, and the lysate was serially diluted using 0.05% Tween-80 in PBS. The diluted lysate was plated on 7H10 agar plates and incubated at 37 ºC for 3-4 weeks. Colonies were counted, and CFUs per well were calculated.

Phagosome-lysosome fusion assay

Differentiated THP-1 cells were plated at $4x10^4$ cells per well in an 8-well Millicell EZ slide (Sigma) and then infected with mEmerald-expressing *M. tuberculosis* mc^26206 at an MOI of 10:1 (macrophages:bacteria) for 4 hrs. 100 nM Lysotracker (Thermo Fisher) was added for the last hour of infection and extracellular bacteria were removed by washing 3-4 times with cold PBS. Cells were then fixed with 4% paraformaldehyde (Fisher Scientific) for 1 hour at RT; washed thrice with

PBS; permeabilized with 0.5% saponin in PBS; washed thrice with PBS. 30 µl of VECTASHIELD® with DAPI was added to each well. The slide was mounted with a coverslip and sealed with nail polish. Fusion of *M. tuberculosis*-containing phagosomes with lysosomes was quantified by blinded assessment of colocalization of mEmerald with Lysotracker using a Nikon TiE A1R-SIMe confocal microscope.

VAMP2 spatial distribution

iBMDMs expressing eGFP-VAMP2 were plated at $4x10^4$ cells per well in an 8-well Millicell EZ slide (Sigma) then infected with mCherry-expressing *M. tuberculosis* mc^26206 at an MOI of 10:1 (macrophages:bacteria) for 4 hrs. As described in "*Phagosome-lysosome fusion assay*", extracellular bacteria were washed and iBMDMs were fixed with 4% paraformaldehyde. Cells were then permeabilized and slides were mounted using VECTASHIELD® with DAPI. Images of infected and uninfected macrophages were acquired using a Nikon TiE A1R-SIMe confocal microscope.

Acknowledgments

We thank Ms. Emily Lopes for help with blinding and Drs. Alissa Rothchild, Shumin Tan, and Hesper Rego for valuable discussion and protocols. We also thank the directors of the University of Massachusetts Amherst Mass Spectrometry, Light Microscopy, and Flow Cytometry facilities Drs. Stephen Eyles, James Chambers, and Amy Burnside for their help and advice. These studies were supported by the National Institute of Allergy and Infectious Diseases (R21AI163949 to M.S.S. and B.M.S.) and the National Science Foundation (2320737 and 2117338 to B.M.S.). Figures created with BioRender.com.

References

1. D. E. Minnikin, Chemical principles in the organization of lipid components in the mycobacterial cell envelope. *Res. Microbiol.* **142**, 423–427 (1991).
2. J. K. Actor, "Trehalose Dimycolate (Cord Factor) as a Contributing Factor to Tuberculosis Pathogenesis" in *Tuberculosis Host-Pathogen Interactions*, J. D. Cirillo, Y. Kong, Eds. (Springer International Publishing, 2019), pp. 43–61.
3. E. Ishikawa, *et al.*, Direct recognition of the mycobacterial glycolipid, trehalose dimycolate, by C-type lectin Mincle. *J. Exp. Med.* **206**, 2879–2888 (2009).
4. I. Matsunaga, D. B. Moody, Mincle is a long sought receptor for mycobacterial cord factor. *J. Exp. Med.* **206**, 2865–2868 (2009).
5. H. Schoenen, *et al.*, Cutting Edge: Mincle Is Essential for Recognition and Adjuvanticity of the Mycobacterial Cord Factor and its Synthetic Analog Trehalose-Dibehenate. *J. Immunol.* **184**, 2756–2760 (2010).
6. E. C. Patin, *et al.*, Trehalose dimycolate interferes with FcγR-mediated phagosome maturation through Mincle, SHP-1 and FcγRIIB signalling. *PLOS ONE* **12**, e0174973 (2017).
7. J. Indrigo, R. L. Hunter, J. K. Actor, Cord factor trehalose 6,6′-dimycolate (TDM) mediates trafficking events during mycobacterial infection of murine macrophages. *Microbiology* **149**, 2049–2059 (2003).
8. J. M. Blander, R. Medzhitov, On regulation of phagosome maturation and antigen presentation. *Nat. Immunol.* **7**, 1029–1035 (2006).
9. A.-M. Pauwels, M. Trost, R. Beyaert, E. Hoffmann, Patterns, Receptors, and Signals: Regulation of Phagosome Maturation. *Trends Immunol.* **38**, 407–422 (2017).
10. J. A. Armstrong, P. D. Hart, RESPONSE OF CULTURED MACROPHAGES TO *MYCOBACTERIUM TUBERCULOSIS* , WITH OBSERVATIONS ON FUSION OF LYSOSOMES WITH PHAGOSOMES. *J. Exp. Med.* **134**, 713–740 (1971).
11. J. Augenstreich, V. Briken, Host Cell Targets of Released Lipid and Secreted Protein Effectors of Mycobacterium tuberculosis. *Front. Cell. Infect. Microbiol.* **10**, 595029 (2020).

12. I. Vergne, *et al.*, *Mycobacterium tuberculosis* Phagosome Maturation Arrest: Mycobacterial Phosphatidylinositol Analog Phosphatidylinositol Mannoside Stimulates Early Endosomal Fusion. *Mol. Biol. Cell* **15**, 751–760 (2004).
13. R. A. Fratti, J. Chua, V. Deretic, Cellubrevin alterations and Mycobacterium tuberculosis phagosome maturation arrest. *J. Biol. Chem.* **277**, 17320–17326 (2002).
14. R. A. Fratti, J. Chua, I. Vergne, V. Deretic, Mycobacterium tuberculosis glycosylated phosphatidylinositol causes phagosome maturation arrest. *Proc. Natl. Acad. Sci. U. S. A.* **100**, 5437–5442 (2003).
15. B. J. Spargo, L. M. Crowe, T. Ioneda, B. L. Beaman, J. H. Crowe, Cord factor (alpha,alpha-trehalose 6,6'-dimycolate) inhibits fusion between phospholipid vesicles. *Proc. Natl. Acad. Sci.* **88**, 737–740 (1991).
16. W. L. Beatty, *et al.*, Trafficking and Release of Mycobacterial Lipids from Infected Macrophages. *Traffic* **1**, 235–247 (2000).
17. E. Rhoades, *et al.*, Identification and macrophage-activating activity of glycolipids released from intracellular *Mycobacterium bovis* BCG. *Mol. Microbiol.* **48**, 875–888 (2003).
18. R. E. Geisel, K. Sakamoto, D. G. Russell, E. R. Rhoades, In Vivo Activity of Released Cell Wall Lipids of *Mycobacterium bovis* Bacillus Calmette-Guérin Is Due Principally to Trehalose Mycolates. *J. Immunol.* **174**, 5007–5015 (2005).
19. C. Cambier, S. M. Banik, J. A. Buonomo, C. R. Bertozzi, Spreading of a mycobacterial cell-surface lipid into host epithelial membranes promotes infectivity. *eLife* **9**, e60648 (2020).
20. I. Dingjan, *et al.*, Endosomal and Phagosomal SNAREs. *Physiol. Rev.* **98**, 1465–1492 (2018).
21. J. G. Duman, J. G. Forte, What is the role of SNARE proteins in membrane fusion? *Am. J. Physiol. Cell Physiol.* **285**, C237-249 (2003).
22. T. O. Omotade, C. R. Roy, Manipulation of Host Cell Organelles by Intracellular Pathogens. *Microbiol. Spectr.* **7** (2019).
23. R. Chatterjee, S. R. G. Setty, D. Chakravortty, SNAREs: a double-edged sword for intravacuolar bacterial pathogens within host cells. *Trends Microbiol.* **32**, 477–493 (2024).
24. H. Yamagami, *et al.*, Trehalose 6,6′-Dimycolate (Cord Factor) of *Mycobacterium tuberculosis* Induces Foreign-Body- and Hypersensitivity-Type Granulomas in Mice. *Infect. Immun.* **69**, 810–815 (2001).
25. J. I. Moliva, J. Turner, J. B. Torrelles, Immune Responses to Bacillus Calmette–Guérin Vaccination: Why Do They Fail to Protect against Mycobacterium tuberculosis? *Front. Immunol.* **8** (2017).
26. W. Antonin, A SNARE complex mediating fusion of late endosomes defines conserved properties of SNARE structure and function. *EMBO J.* **19**, 6453–6464 (2000).
27. P. R. Pryor, *et al.*, Combinatorial SNARE complexes with VAMP7 or VAMP8 define different late endocytic fusion events. *EMBO Rep.* **5**, 590–595 (2004).
28. F. Deák, S. Schoch, X. Liu, T. C. Südhof, E. T. Kavalali, Synaptobrevin is essential for fast synaptic-vesicle endocytosis. *Nat. Cell Biol.* **6**, 1102–1108 (2004).
29. L. Gómez-Jaramillo, *et al.*, VAMP2 is implicated in the secretion of antibodies by human plasma cells and can be replaced by other synaptobrevins. *Cell. Mol. Immunol.* **15**, 353–366 (2018).
30. S. Axelrod, *et al.*, Delay of phagosome maturation by a mycobacterial lipid is reversed by nitric oxide. *Cell. Microbiol.* **10**, 1530–1545 (2008).
31. I. Vergne, J. Chua, V. Deretic, Tuberculosis Toxin Blocking Phagosome Maturation Inhibits a Novel Ca2+/Calmodulin-PI3K hVPS34 Cascade. *J. Exp. Med.* **198**, 653–659 (2003).
32. R. A. Fratti, J. M. Backer, J. Gruenberg, S. Corvera, V. Deretic, Role of phosphatidylinositol 3-kinase and Rab5 effectors in phagosomal biogenesis and mycobacterial phagosome maturation arrest. *J. Cell Biol.* **154**, 631–644 (2001).
33. H. W. Kavunja, *et al.*, Photoactivatable Glycolipid Probes for Identifying Mycolate–Protein Interactions in Live Mycobacteria. *J. Am. Chem. Soc.* **142**, 7725–7731 (2020).
34. J. Ostrop, *et al.*, Contribution of MINCLE–SYK Signaling to Activation of Primary Human APCs by Mycobacterial Cord Factor and the Novel Adjuvant TDB. *J. Immunol.* **195**, 2417–2428 (2015).

35. S. J. Lord, K. B. Velle, R. D. Mullins, L. K. Fritz-Laylin, SuperPlots: Communicating reproducibility and variability in cell biology. *J. Cell Biol.* **219**, e202001064 (2020).
36. L. Gandino, L. Varesio, Immortalization of macrophages from mouse bone marrow and fetal liver. *Exp. Cell Res.* **188**, 192–198 (1990).
37. Y. Liao, J. Wang, E. J. Jaehnig, Z. Shi, B. Zhang, WebGestalt 2019: gene set analysis toolkit with revamped UIs and APIs. *Nucleic Acids Res.* **47**, W199–W205 (2019).
38. D. Szklarczyk, *et al.*, The STRING database in 2023: protein–protein association networks and functional enrichment analyses for any sequenced genome of interest. *Nucleic Acids Res.* **51**, D638–D646 (2023).
39. K. M. S. Misura, L. C. Gonzalez, A. P. May, R. H. Scheller, W. I. Weis, Crystal Structure and Biophysical Properties of a Complex between the N-terminal SNARE Region of SNAP25 and Syntaxin 1a. *J. Biol. Chem.* **276**, 41301–41309 (2001).
40. D. Brandhorst, *et al.*, Homotypic fusion of early endosomes: SNAREs do not determine fusion specificity. *Proc. Natl. Acad. Sci.* **103**, 2701–2706 (2006).
41. S. J. Williams, Sensing Lipids with Mincle: Structure and Function. *Front. Immunol.* **8**, 1662 (2017).
42. H. G. Tima, *et al.*, Inflammatory Properties and Adjuvant Potential of Synthetic Glycolipids Homologous to Mycolate Esters of the Cell Wall of Mycobacterium tuberculosis. *J. Innate Immun.* **9**, 162–180 (2017).
43. A. Decout, *et al.*, Rational design of adjuvants targeting the C-type lectin Mincle. *Proc. Natl. Acad. Sci.* **114**, 2675–2680 (2017).
44. T. Rowe, C. Dascher, S. Bannykh, H. Plutner, W. E. Balch, Role of Vesicle-Associated Syntaxin 5 in the Assembly of Pre-Golgi Intermediates. *Science* **279**, 696–700 (1998).
45. K. Arasaki, D. K. Toomre, C. R. Roy, The Legionella pneumophila Effector DrrA Is Sufficient to Stimulate SNARE-Dependent Membrane Fusion. *Cell Host Microbe* **11**, 46–57 (2012).
46. T. Kitao, *et al.*, Legionella Manipulates Non-canonical SNARE Pairing Using a Bacterial Deubiquitinase. *Cell Rep.* **32**, 108107 (2020).
47. H. Warner, S. Mahajan, G. Van Den Bogaart, Rerouting trafficking circuits through posttranslational SNARE modifications. *J. Cell Sci.* **135**, jcs260112 (2022).
48. J. Suzuki, *et al.*, Involvement of Syntaxin 7 in Human Gastric Epithelial Cell Vacuolation Induced by the Helicobacter pylori-produced Cytotoxin VacA. *J. Biol. Chem.* **278**, 25585–25590 (2003).
49. P. K. Singh, *et al.*, *Salmonella* SipA mimics a cognate SNARE for host Syntaxin8 to promote fusion with early endosomes. *J. Cell Biol.* **217**, 4199–4214 (2018).
50. D.-C. Bui, L. M. Jorgenson, S. P. Ouellette, E. A. Rucks, Eukaryotic SNARE VAMP3 Dynamically Interacts with Multiple Chlamydial Inclusion Membrane Proteins. *Infect. Immun.* **89**, e00409-20 (2021).
51. S. Martinez-Arca, *et al.*, A dual mechanism controlling the localization and function of exocytic v-SNAREs. *Proc. Natl. Acad. Sci.* **100**, 9011–9016 (2003).
52. J. A. Armstrong, P. D. Hart, Phagosome-lysosome interactions in cultured macrophages infected with virulent tubercle bacilli. Reversal of the usual nonfusion pattern and observations on bacterial survival. *J. Exp. Med.* **142**, 1–16 (1975).
53. S. Sturgill-Koszycki, *et al.*, Lack of Acidification in *Mycobacterium* Phagosomes Produced by Exclusion of the Vesicular Proton-ATPase. *Science* **263**, 678–681 (1994).
54. D. L. Clemens, M. A. Horwitz, Characterization of the Mycobacterium tuberculosis phagosome and evidence that phagosomal maturation is inhibited. *J. Exp. Med.* **181**, 257–270 (1995).
55. S. Cheng, C. Sun, W. Lao, H. Kang, Association of *VAMP8* rs1010 Polymorphism with Host Susceptibility to Pulmonary Tuberculosis in a Chinese Han Population. *Genet. Test. Mol. Biomark.* **23**, 299–303 (2019).
56. W. Yu, J. M. Baskin, Photoaffinity labeling approaches to elucidate lipid–protein interactions. *Curr. Opin. Chem. Biol.* **69**, 102173 (2022).
57. C. Schultz, Chemical Tools for Lipid Cell Biology. *Acc. Chem. Res.* **56**, 1168–1177 (2023).

58. J. L. Babulic, F. V. De León González, C. J. Capicciotti, Recent advances in photoaffinity labeling strategies to capture Glycan–Protein interactions. *Curr. Opin. Chem. Biol.* **80**, 102456 (2024).
59. E. Lesur, *et al.*, First access to a mycolic acid-based bioorthogonal reporter for the study of the mycomembrane and mycoloyltransferases in Corynebacteria. *Chem. Commun. Camb. Engl.* **55**, 13074–13077 (2019).
60. C. Labarre, *et al.*, Bioorthogonal Monomycolate of Trehalose Disclosed the O-Mycoloylation of Mycoloyltransferases and Other Cell Envelope Proteins in C. glutamicum. *ACS Chem. Biol.* (2024). https://doi.org/10.1021/acschembio.4c00502.
61. A. Sut, *et al.*, Mycobacteria glycolipids as potential pathogenicity effectors: alteration of model and natural membranes. *Biochemistry* **29**, 8498–8502 (1990).
62. M. Mishra, R. Dadhich, P. Mogha, S. Kapoor, Mycobacterium Lipids Modulate Host Cell Membrane Mechanics, Lipid Diffusivity, and Cytoskeleton in a Virulence-Selective Manner. *ACS Infect. Dis.* **6**, 2386–2399 (2020).
63. T. Lang, SNARE proteins and 'membrane rafts.' *J. Physiol.* **585**, 693–698 (2007).
64. C. Wang, *et al.*, Different regions of synaptic vesicle membrane regulate VAMP2 conformation for the SNARE assembly. *Nat. Commun.* **11**, 1531 (2020).
65. Z. Fezoua-Boubegtiten, *et al.*, The transmembrane domain of the SNARE protein VAMP2 is highly sensitive to its lipid environment. *Biochim. Biophys. Acta BBA - Biomembr.* **1861**, 670–676 (2019).
66. W. Wickner, Membrane Fusion: Five Lipids, Four SNAREs, Three Chaperones, Two Nucleotides, and a Rab, All Dancing in a Ring on Yeast Vacuoles. *Annu. Rev. Cell Dev. Biol.* **26**, 115–136 (2010).
67. A. Sardar, N. Dewangan, B. Panda, D. Bhowmick, P. K. Tarafdar, Lipid and Lipidation in Membrane Fusion. *J. Membr. Biol.* **255**, 691–703 (2022).
68. N. Vashi, S. B. A. Andrabi, S. Ghanwat, M. Suar, D. Kumar, Ca2+-dependent Focal Exocytosis of Golgi-derived Vesicles Helps Phagocytic Uptake in Macrophages. *J. Biol. Chem.* **292**, 5144–5165 (2017).
69. E. Layre, Trafficking of Mycobacterium tuberculosis Envelope Components and Release Within Extracellular Vesicles: Host-Pathogen Interactions Beyond the Wall. *Front. Immunol.* **11**, 1230 (2020).
70. W. L. Beatty, H.-J. Ullrich, D. G. Russell, Mycobacterial surface moieties are released from infected macrophages by a constitutive exocytic event. *Eur. J. Cell Biol.* **80**, 31–40 (2001).
71. P. Pancholi, A. Mirza, N. Bhardwaj, R. M. Steinman, Sequestration From Immune CD4 $^{+}$ T Cells of Mycobacteria Growing in Human Macrophages. *Science* **260**, 984–986 (1993).
72. C. R. Singh, *et al.*, Processing and Presentation of a Mycobacterial Antigen 85B Epitope by Murine Macrophages Is Dependent on the Phagosomal Acquisition of Vacuolar Proton ATPase and In Situ Activation of Cathepsin D. *J. Immunol.* **177**, 3250–3259 (2006).
73. H. Soualhine, *et al.*, *Mycobacterium bovis* Bacillus Calmette-Guérin Secreting Active Cathepsin S Stimulates Expression of Mature MHC Class II Molecules and Antigen Presentation in Human Macrophages. *J. Immunol.* **179**, 5137–5145 (2007).
74. C. Jagannath, *et al.*, Autophagy enhances the efficacy of BCG vaccine by increasing peptide presentation in mouse dendritic cells. *Nat. Med.* **15**, 267–276 (2009).
75. S. L. Sampson, *et al.*, Protection Elicited by a Double Leucine and Pantothenate Auxotroph of *Mycobacterium tuberculosis* in Guinea Pigs. *Infect. Immun.* **72**, 3031–3037 (2004).

Figures

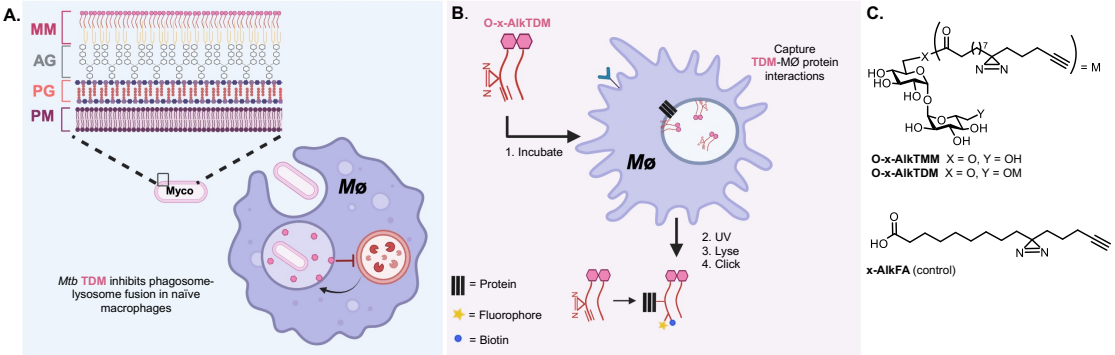

Figure 1. Chemical probes as tools to understand how (myco)bacterial lipids interact with host cells. (A) The glycolipid trehalose dimycolate (TDM) in the outer mycomembrane (MM) of *Mycobacterium tuberculosis* (*Mtb*) inhibits fusion of lysosomes with *M. tuberculosis*-containing phagosomes. Other components of the mycobacterial cell envelope include arabinogalactan (AG), peptidoglycan (PG), and the inner plasma membrane (PM). (B) Workflow for chemical proteomics using the TDM-mimicking probe O-x-AlkTDM. (C) Structures of O-x-AlkTDM and control probes O-x-AlkTMM and x-AlkFA.

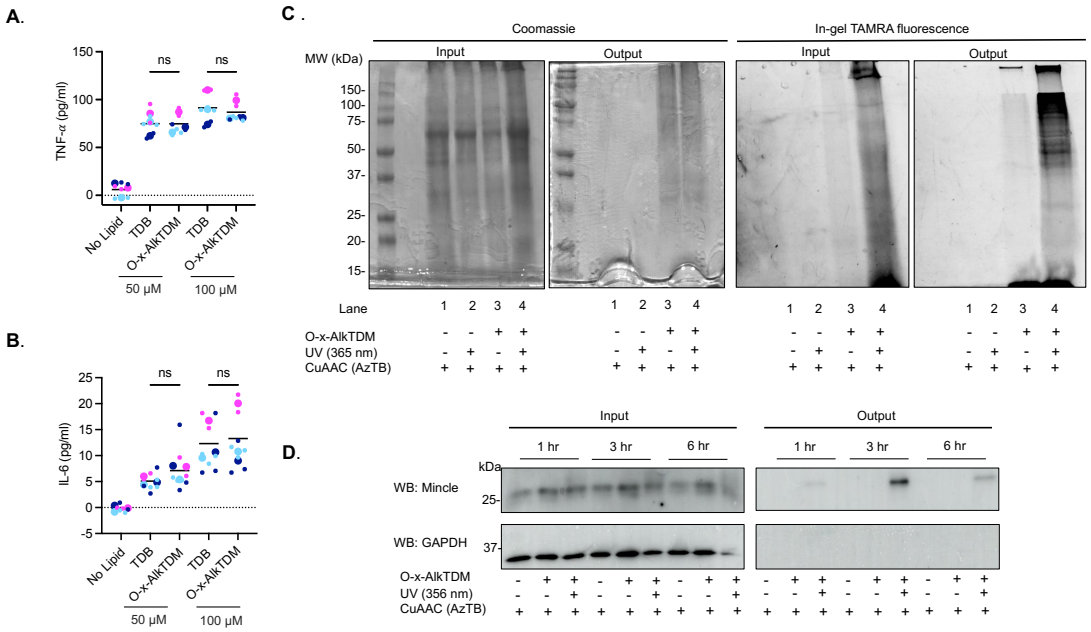

Figure 2. Mycobacterial glycolipid probe O-x-AlkTDM recapitulates TDM activity and binding in macrophages. ELISA detection of pro-inflammatory cytokines (A) TNF-α and (B) IL-6 after 6 hr incubation of immortalized bone marrow-derived macrophages (iBMDMs) from C57BL/6 mice with O-x-AlkTDM or commercial TDM mimic trehalose dibehenate (TDB). For (A-B) each color in the SuperPlots (35) represents an independent biological replicate. Smaller symbols represent technical replicates, and larger symbols are the means of the technical replicates for each independent experiment. Statistical significance determined using a two-way ANOVA with a Šídák's multiple comparisons test for post hoc analysis. Data were obtained from three independent experiments (A-B). (C) O-x-AlkTDM-mediated affinity enrichment of host interacting proteins. iBMDMs were incubated with O-x-AlkTDM (100 μM), UV-irradiated, and lysed. Lysates were reacted with TAMRA Biotin Azide (AzTB) via copper-catalyzed alkyne-azide cycloaddition (CuAAC) and analyzed by Coomassie and in-gel TAMRA fluorescence (input). Clicked samples were incubated with NeutrAvidin agarose beads (output) to evaluate global enrichment of proteins (C) and specific enrichment of the known TDM receptor Mincle (D). Representative data shown for three independent biological replicates (C-D).

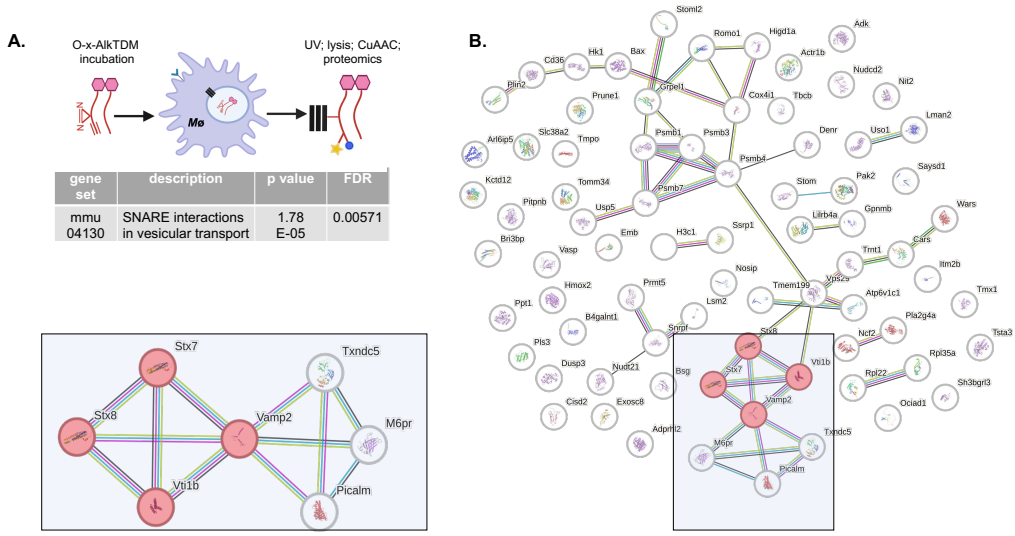

gene set	description	p value	FDR
mmu 04130	SNARE interactions in vesicular transport	1.78 E-05	0.00571

Figure 3. Chemical proteomics identifies SNAREs as putative O-x-AlkTDM-interacting proteins. (A) iBMDMs were incubated +/- O-x-alkTDM for 6 hrs; exposed to UV or not; lysed; and subjected to CuAAC with AzTB as in Figure 2C-D. O-x-AlkTDM-interacting proteins were then enriched by NeutrAvidin agarose beads; digested with trypsin; and analyzed by LC-MS/MS. Over-Representation Analysis (ORA) performed via WEBGestalt (37). Cut-off set at $p<0.05$ and false discovery rate (FDR)<0.25. Enrichment is relative to no-probe samples across four independent biological replicates for each sample. (B) STRING (Search Tool for Retrieval of Interacting Genes/Proteins) network analysis (38) shows functional associations of proteins identified in (A). Intra-network interactions between SNARE proteins (red) are shown by the connected lines.

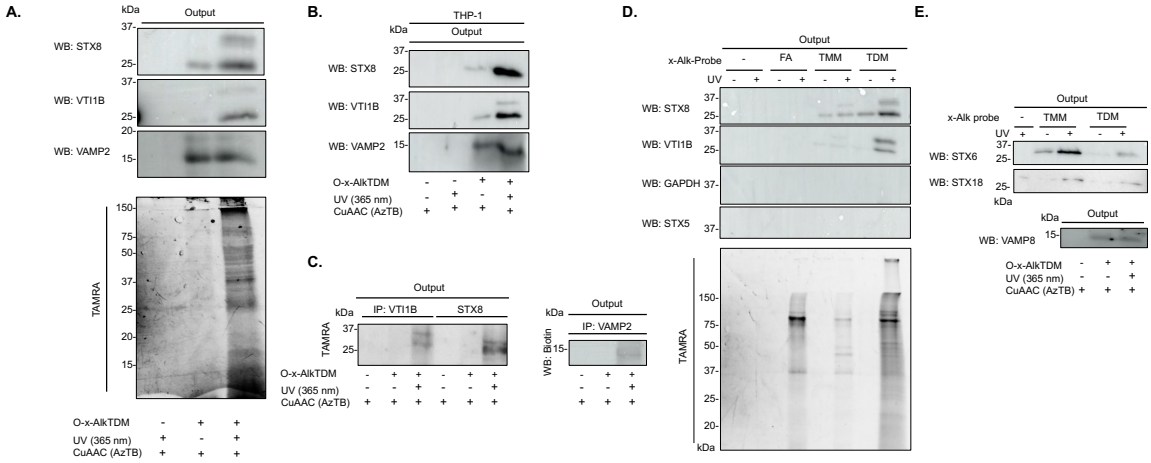

Figure 4. Macrophage SNAREs interact with O-x-AlkTDM. iBMDMs (A) or THP-1s (B) were treated 6 hrs +/- O-x-AlkTDM and processed as in Figure 2C-D. Interacting proteins detected by in-gel fluorescence (TAMRA) or by Western blotting using the indicated anti-SNARE antibodies. (C) iBMDMs treated as in (A) but immunoprecipitated using the indicated anti-SNARE antibody. The presence of O-x-AlkTDM was confirmed by in-gel fluorescence (TAMRA) or Western blotting using anti-biotin. (D) Probes (Figure 1C) that lack a lipid chain (O-x-AlkTMM) or trehalose (x-AlkFA) respectively interact poorly or not at all with SNAREs. iBMDMs were treated or not with the different probes for 6 hrs and processed as in (A). x-Alk probe-interacting proteins were also probed for the presence of the SNARE STX5 and the housekeeping protein GAPDH. (E) O-x-AlkTDM interacts with SNAREs beyond those identified by chemical proteomics. iBMDMs were treated and processed as in (A). Expression data from lysates for (D-E) available in SI, Figure S6. Double bands likely SNAREs interacting with one or two molecules of probe (SI, Figure S5). Representative data shown for 2-5 independent biological replicates.

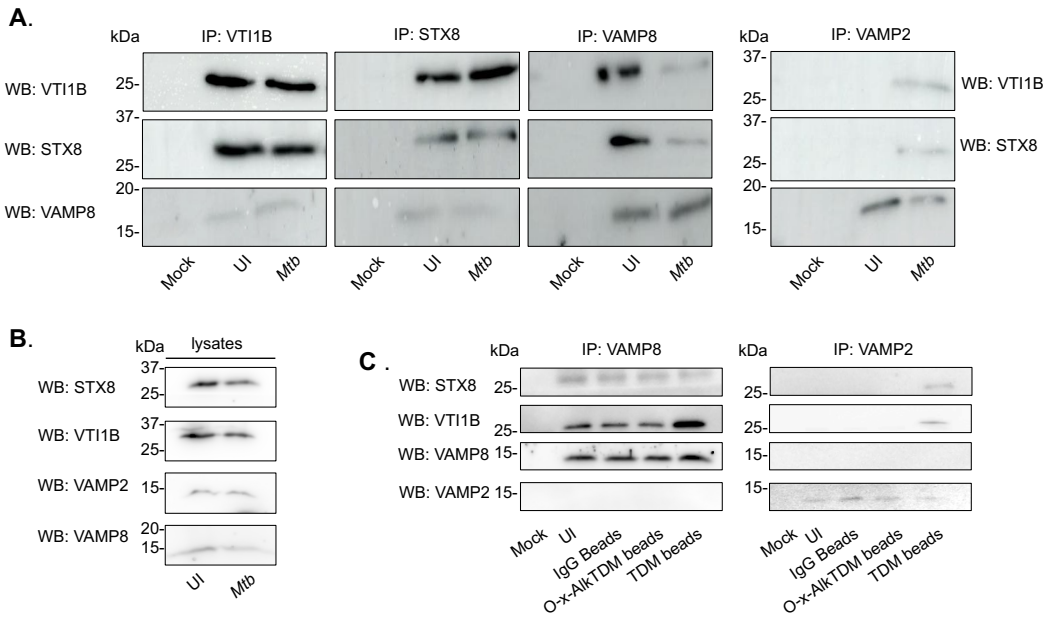

Figure 5. Non-canonical SNARE complexation is triggered by *M. tuberculosis* (*Mtb*) or native TDM. (A) iBMDMs were infected +/- *M. tuberculosis* (MOI 1:50 macrophages:bacteria) then immunoprecipitated and immunoblotted with indicated anti-SNARE antibodies. The VTI1B-STX8 interaction is *M. tuberculosis*-independent, whereas VAMP2 and VAMP8 interactions with VTI1B-STX8 occur preferentially when *M. tuberculosis* is present or absent, respectively. (B) SNARE expression +/- *M. tuberculosis*. iBMDMs infected as in (A) and lysates (10 µg/lane) were immunoblotted with indicated anti-SNARE antibodies. (C) iBMDMs were incubated +/- latex beads coated with IgG, O-x-AlkTDM, or native TDM (1:50 macrophages:bead) then processed as in (A). Native TDM is sufficient to trigger VAMP2 interaction with VTI1B and STX8, although a concomitant change in VAMP8 interactions with these proteins was not detected. Mock, isotype control for each primary antibody. UI, uninfected (A-B) or unincubated (C). Representative data shown for 2-3 independent biological replicates.

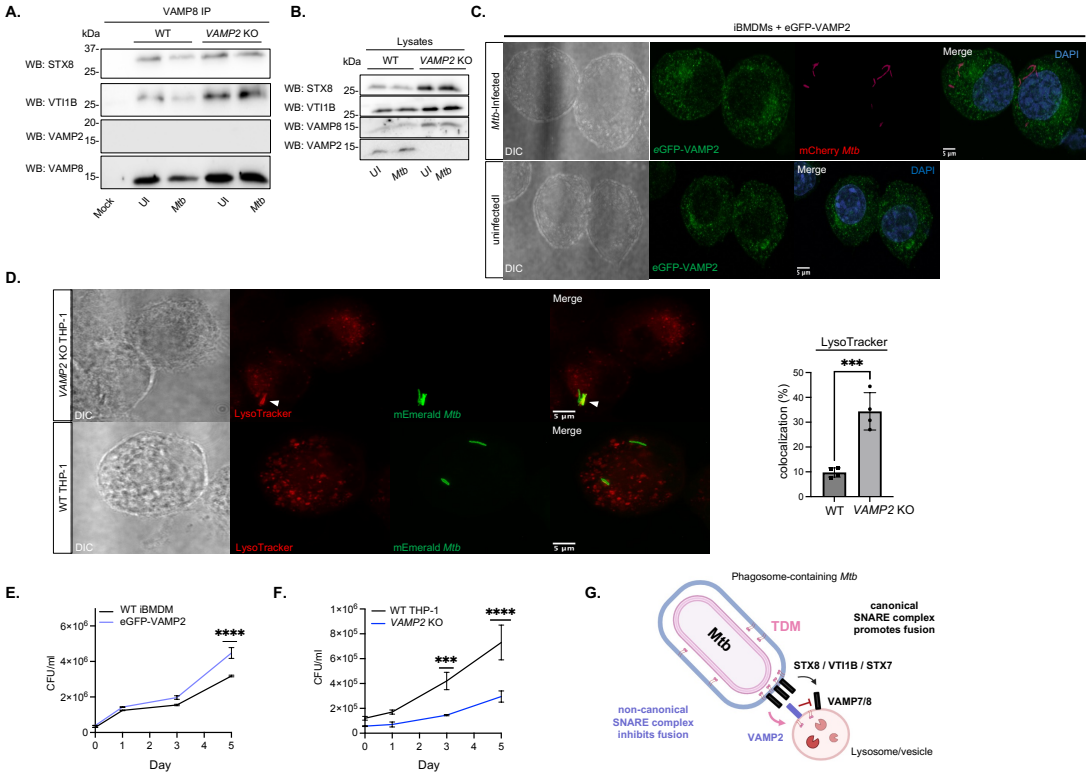

Figure 6. VAMP2 inhibits phagosome-lysosome fusion and promotes *M. tuberculosis* survival during macrophage infection. WT and *VAMP2* knockout THP-1s were infected +/- *M. tuberculosis* (MOI 1:50 macrophages:bacteria) and immunoblotted with anti-SNAREs after (A) or before (B) immunoprecipitation. VAMP8 complexation with VTI1B and STX8 in the presence of *M. tuberculosis* is enhanced in the absence of VAMP2. An independent biological replicate is included for comparison in SI, Figure S8. Mock, isotype control for each primary antibody. UI, uninfected. (C) iBMDMs expressing eGFP-VAMP2 were infected +/- mCherry-expressing *M. tuberculosis* (MOI 1:10, macrophages:bacteria). (D) Loss of *VAMP2* is associated with enhanced phagosome-lysosome fusion. THP-1s were infected with mEmerald-expressing *M. tuberculosis* as in (A). Representative images show spatial coincidence between *M. tuberculosis* and lysosomal compartments, which were stained with LysoTracker in WT and *VAMP2* knockout THP-1 cells. Blinded quantification, right, from four independent biological replicates ranging from n=13-26 individual bacteria per sample. Statistical significance was determined using unpaired Student's t test. (E-F) VAMP2 expression correlates with *M. tuberculosis* survival. iBMDMs expressing eGFP-VAMP2 (and overexpressing VAMP2; SI, Figure S7) or not (E) and wild-type and *VAMP2* knockout THP-1s (F) were infected +/- *M. tuberculosis* (MOI 1:10, macrophages:bacteria). Macrophages were lysed and plated for colony-forming units at the indicated time points after infection. Representative data shown for 2-3 independent biological replicates. Statistical significance was determined using a two-way ANOVA with a Šídák's multiple comparisons test for post hoc analysis. (G) Proposed model for TDM-SNARE interactions. TDM released from the mycomembrane of *M. tuberculosis* (Figure 1A) intercalates into macrophage membranes, including the those of the phagosome and other vesicles. The altered membrane milieux promote non-canonical, VAMP2-containing SNARE complexation at the expense of canonical, VAMP8-containing SNARE complexation. Fusion of lysosomes with the *M. tuberculosis*-containing phagosome is directly or indirectly suppressed, enabling the pathogen to evade destruction by naïve macrophages.

Supplementary Materials and Methods

General experimental for synthesis. Reagents and solvents were procured from commercial sources without further purification unless otherwise noted. Anhydrous solvents were obtained either commercially or from an alumina column solvent purification system. All reactions were carried out in oven-dried glassware under inert gas unless otherwise noted. Analytical thin-layer chromatography (TLC) was performed on glass-backed silica gel 60 Å plates (thickness 250 µm) and detected by charring with 5% H_2SO_4 in EtOH. Column chromatography was performed using flash-grade silica gel 32–63 µm (230–400 mesh). NMR spectra were obtained using Bruker Avance 500 instrument. Coupling constants (*J*) are reported in hertz (Hz) with chemical shifts in ppm (δ) referenced to solvent peaks, with the following splitting abbreviations: s = singlet, d = doublet, dd = doublet of doublets, ddd = doublet of doublet of doublets, dt = doublet of triplets, t = triplet, td = triplet of doublets, m = multiplet. High-resolution electrospray ionization (HR ESI) mass spectra were obtained using an Agilent 6545XT LC-ESI-MS QTOF instrument.

Synthesis of O-x-AlkTDM. Synthesis of O-x-AlkTDM was adapted from a previously reported procedure.[1] An oven-dried round-bottom flask was charged with *N*,*N*'-dicyclohexylcarbodiimide (DCC) (0.207 g, 1.00 mmol) and *N*,*N*-dimethylamino-4-pyridine (DMAP) (0.063 g, 0.516 mmol). After drying the reagents under high vacuum and placing the flask under an argon atmosphere, anhydrous CH_2Cl_2 (5 mL) was added, and the mixture was cooled to 0 °C. To the stirring solution was added 9-(3-pent-4-ynyl-3-H-diazirin-3-yl-nonanoic acid[1] (0.201 g, 0.760 mmol dissolved in 0.5 mL anhydrous CH_2Cl_2) and the reaction was stirred for 30 min. This was followed by slow, dropwise addition of freshly prepared solution of 2, 3, 4, 2', 3', 4'-hexakis-*O*-(trimethylsilyl)-α,α-trehalose[1] (0.384 g, 0.495 mmol) in anhydrous CH_2Cl_2 (5 mL). The reaction mixture was stirred and gradually allowed to warm to room temperature. After TLC (hexanes/ethyl acetate 4:1) showed generation of mono- and diester products in approximately equal amounts (approximately 12 h), the reaction was quenched by addition of excess CH_3OH and concentrated by rotary evaporation. The concentrated mixture was purified by silica gel chromatography (4:1 hexanes/ethyl acetate containing 1% Et_3N) to give diester intermediate as an off-white solid. The intermediate was dissolved in CH_3OH (5 mL) and Dowex 50WX8-400H^+ ion-exchange resin was added and stirred for 30 min at room temperature, after which TLC (CH_2Cl_2/CH_3OH 4:1) indicated the reaction was complete. The resin was filtered off and the filtrate was concentrated by rotary evaporation and purified by silica gel chromatography (CH_2Cl_2/CH_3OH 9:1) to give O-x-AlkTDM (0.092 g, 29% over two steps) as a white solid. ^{1}H NMR (500 MHz, CD_3OD, referenced to methanol peak at 3.34 ppm): δ 5.07 (d, *J* = 3.5 Hz, 2 H), 4.39 (dd, *J* = 1.6, 11.9 Hz, 2 H), 4.23 (dd *J* = 5.3, 11.9 Hz, 2 H), 4.04 (ddd, *J* = 1.5, 5.1, 10.0 Hz, 2 H), 3.81 (t, *J* = 9.3 Hz, 2 H), 3.50 (dd, *J* = 3.6, 9.7 Hz, 2 H), 3.36 (t, *J* = 9.4 Hz, 2 H), 2.37 (t, *J* = 7.2 Hz, 4 H), 2.24 (t, *J* = 2.7 Hz, 2 H), 2.18 (dt, *J* = 2.7, 6.9 Hz, 4 H), 1.65 (pent, *J* = 7.0 Hz, 4 H), 1.51 (t, *J* = 5.3 Hz, 2 H), 1.42-1.26 (m, 26 H) 1.16-1.08 (m, 4 H). ^{13}C NMR (125 MHz, CD_3OD, referenced to methanol peak at 49.86 ppm): δ 176.3, 96.0, 85.0, 75.4, 74.0, 72.8, 72.4, 71.0, 65.3, 35.9, 34.7, 33.6, 31.2, 31.11, 31.09, 30.97, 30.1, 26.9, 25.7, 24.9, 19.4. HRMS (ESI-TOF) m/z $[M+Na]^+$ Calcd for $C_{42}H_{66}N_4O_{13}Na$ 857.4520; found 857.4524. Note that the monoester product generated in the esterification step was also obtained and desilylated according to the reported procedure to give O-x-AlkTMM (41% over two steps), which matched literature-reported NMR data (33).

Synthesis of O-x-AlkTMM and x-AlkFA. Synthesized according to literature-reported procedures (33).

BSA photocrosslinking. The labeling procedure was performed on defatted, reduced, and alkylated bovine serum albumin (BSA) prepared as in previously reported procedures.[1] Briefly, BSA was incubated with excess $CHCl_3$ overnight with stirring. After 12 h, BSA was collected by filtration and dried under air. A 10 mg/mL stock solution in water was prepared and diluted to 3.8 mg/ml. Dithiothreitol (DTT) (100 mM stock in 50 mM ammonium bicarbonate solution) was added to a final concentration of 5 mM and the protein was incubated at 56 °C for 20 min in a thermomixer. To reduced BSA, iodoacetamide was added to a final concentration of 16.5 mM (from 550 mM iodoacetamide stock in 50 mM ammonium bicarbonate solution) and incubated at room temperature in the dark for 20 min. To 90 µL aliquots of reduced and alkylated BSA was added 10 µL of previously reported N-x-AlkTMM-C15[1] as positive control or O-x-AlkTDM synthesized here to a final probe concentration of 100 µM, BSA concentration of 2.7 mg/mL, DMSO concentration of 10%. The mixture was incubated at room temperature with mixing for 1 h. The BSA-probe mixtures were split into two equal volumes in 1.5 mL centrifuge tubes. The samples were either exposed to UV irradiation for 15 min or not using a 15-watt 365 nm UV bench lamp (UVP) at a distance of ~2 cm. All six samples were subjected to Cu-catalyze azide-alkyne cycloaddition (CuAAC) using carboxyrhodamine 110 azide (Click Chemistry Tools) (30 µM) in the presence of sodium ascorbate (1.2 mM), copper(II) sulfate (1 mM) and tris(benzyltriazolylmethyl)amine (TBTA) ligand (128 µM), giving a final BSA concentration of 1.95 mg/ml. The reactions were incubated for 1 h at room temperature. Excess CuAAC reagents were removed by sequential addition of 4 volumes of methanol, 1 volume of chloroform, and 3 volumes of water. Samples were briefly vortexed and centrifuged at 18,000 x g for 5 min. The top methanol layer was carefully aspirated to not to disturb protein wafer. 3 volumes of methanol were added, followed by brief vortex and centrifugation at 18,000 x g for 5 min followed by careful aspiration. The resulting protein pellets were dried for 10 min and resuspended in 100 µL water. 20 µg of each sample was analyzed by 4-20% SDS-polyacrylamide gel electrophoresis (BioRad) in a Tris-glycine-SDS running buffer, followed by fluorescence scanning using a Typhoon FLA 7000 (GE Healthcare Life Science) with a 485 excitation and 520 emission filter. The gel was fixed for 15 min (40% ethanol, 10% acetic acid in milliQ water), rinsed once with milliQ water and stained over night with gentle agitation in QC Colloidal Coomassie stain (Bio-Rad). The gel was rinsed with milliQ water until the background was clear and imaged using a ChemiDoc Touch Imaging System (Bio-Rad) and processed by Image Lab software (Bio-Rad).

Supplementary Figures

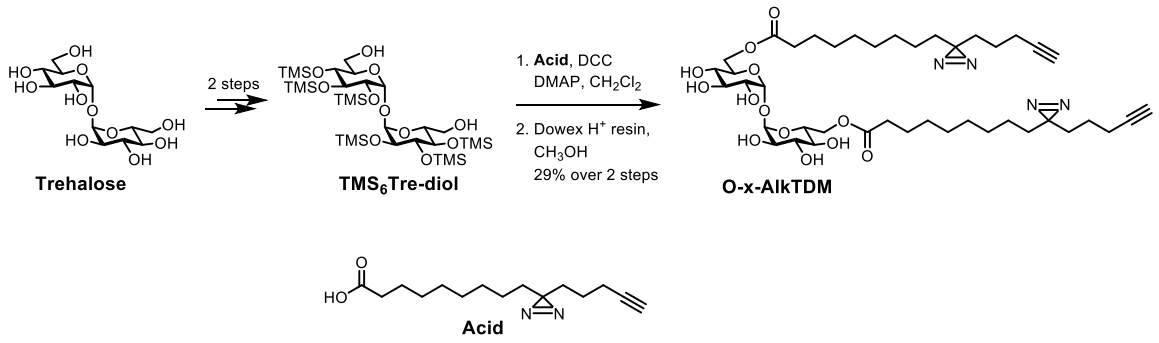

Figure S1. Synthesis of O-x-AlkTDM.

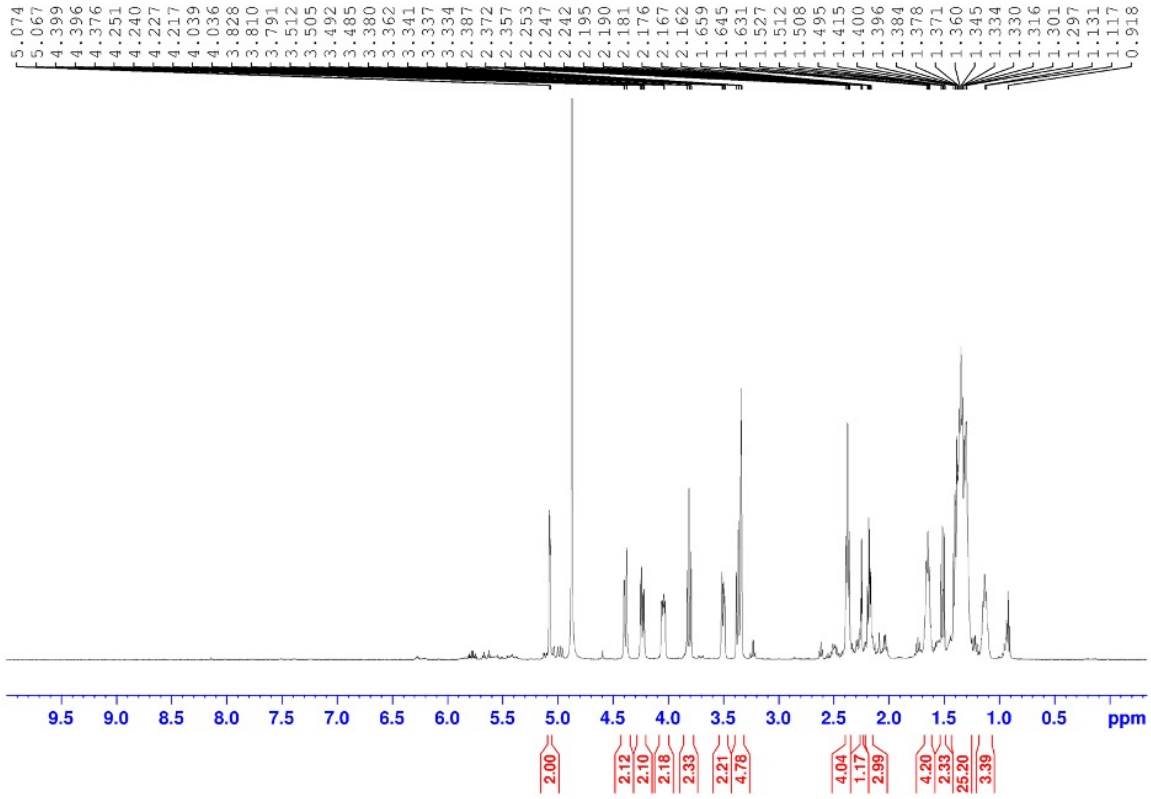

Figure S2. ^{1}H NMR spectrum of O-x-AlkTDM.

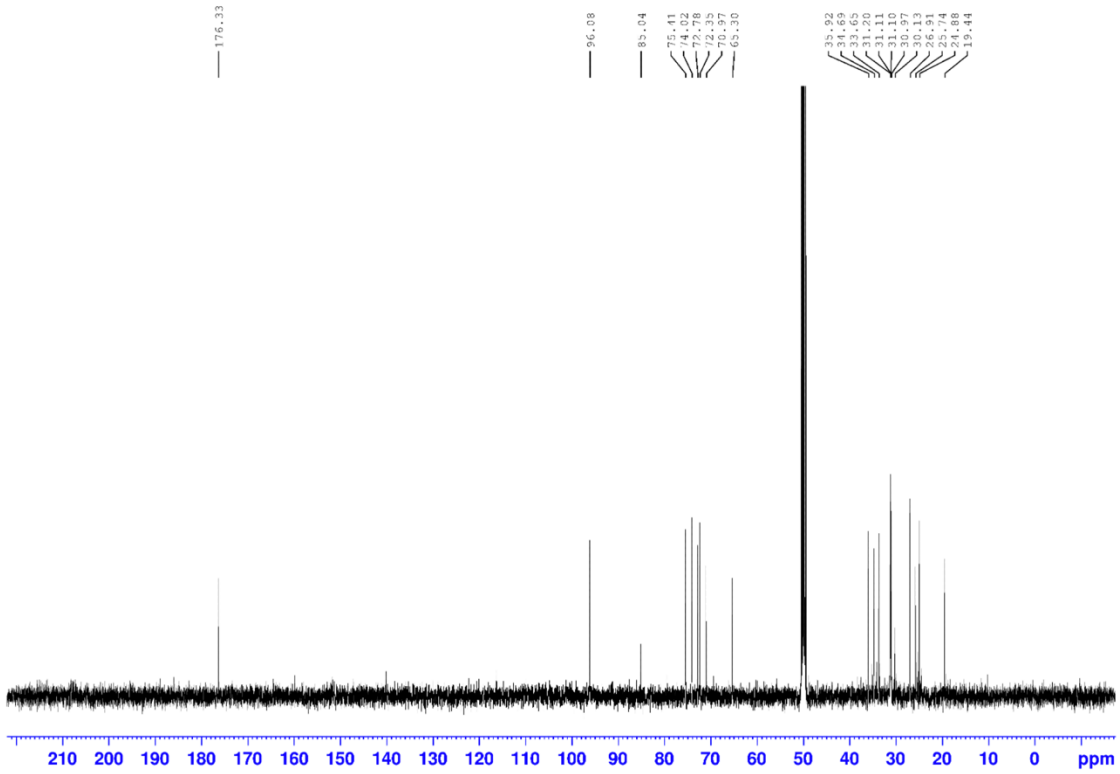

Figure S3. ^{13}C NMR spectrum of O-x-AlkTDM.

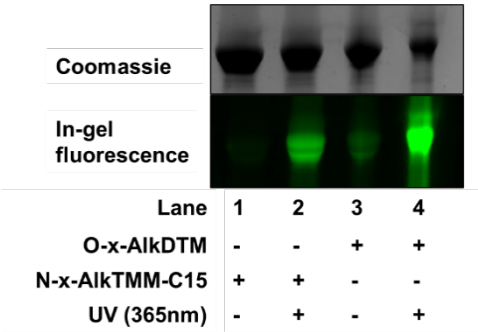

Figure S4. UV-dependent photo-crosslinking of bovine serum albumin (BSA) with O-x-AlkTDM (or positive control N-x-AlkTMM-C15) (33) , followed by CuAAC-mediated fluorescence labeling and SDS-PAGE analysis with fluorescence scanning.

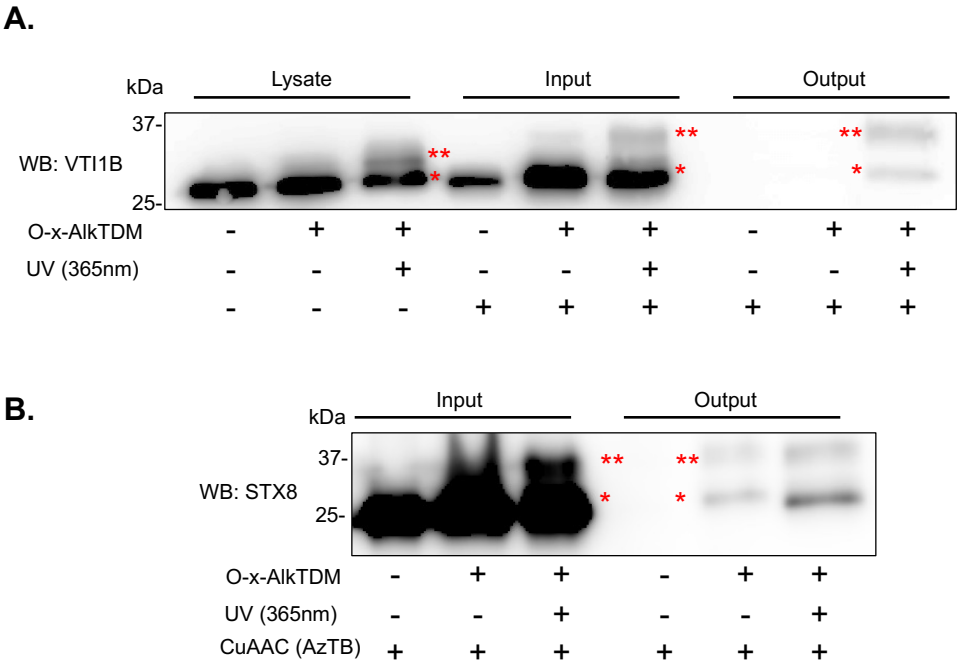

Figure S5. SNAREs may interact with more than one molecule of O-x-AlkTDM probe. iBMDMs were treated 6 hrs +/- O-x-AlkTDM and processed as in Figure 2C-D. Samples were immunoblotted with the indicated antibodies prior to CuAAC (lysates), after CuAAC but prior to affinity purification (input), or after both manipulations (output). The presence of multiple bands (denoted with one or two asterisks), and their apparent increase in size after CuAAC (A), suggest the possibility of one or two O-x-AlkTDM molecules binding per SNARE.

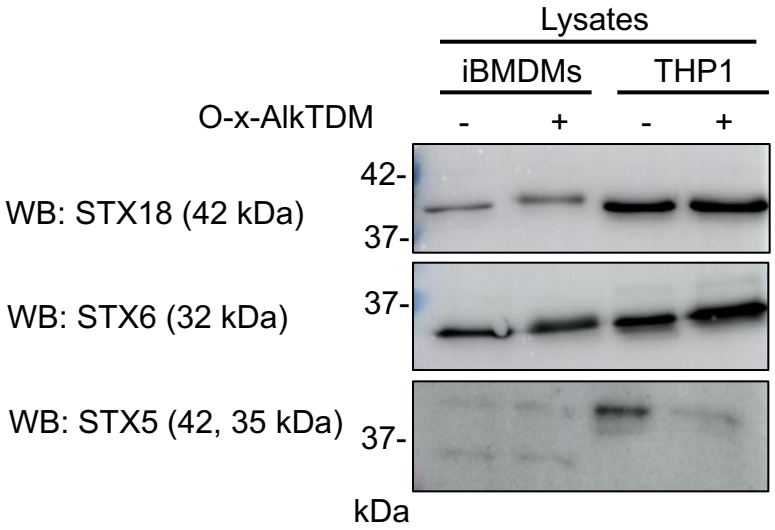

Figure S6. **Detection of various SNAREs in iBMDMs and THP-1s.** Macrophages were incubated +/- O-x-AlkTDM as in Figure 4D-E and lysates were immunoblotted without affinity enrichment.

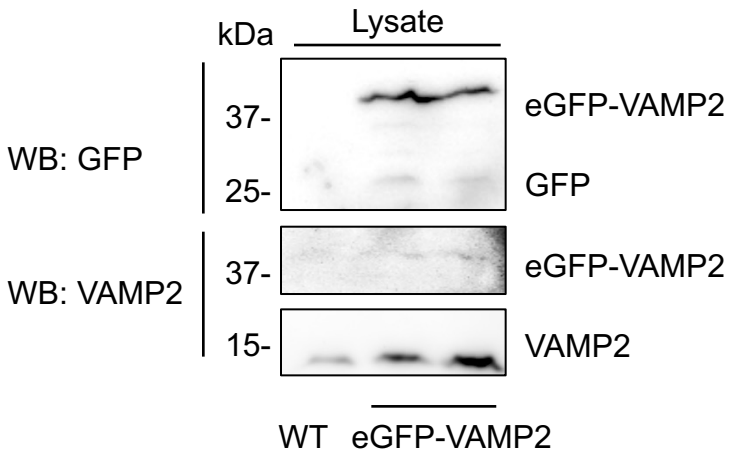

Figure S7. Confirmation of eGFP-VAMP2 expression in iBMDMs. Lysates (20 µg/lane) from WT and eGFP-VAMP2-nucleofected iBMDMs were immunoblotted for GFP and VAMP2. A band at ~40 kDa (VAMP2= 13 kDa and eGFP= 27 kDa) was detected in nucleofected iBMDMs by both antibodies. VAMP2 alone also appears to be overexpressed in these cells (lowest blot).

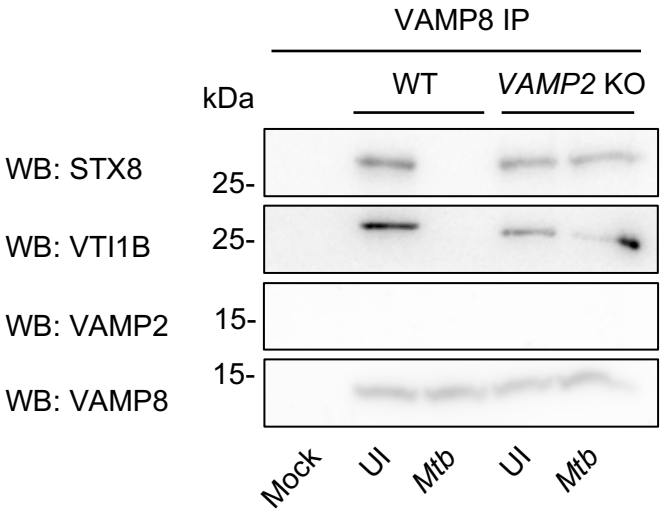

Figure S8. **Independent biological replicate of experiment in Figure 6A.** WT and *VAMP2* knockout THP-1s were infected +/- *M. tuberculosis* (MOI 1:50, macrophages:bacteria) and immunoblotted with anti-SNAREs after immunoprecipitation. VAMP8 complexation with VTI1B and STX8 in the presence of *M. tuberculosis* is rescued in the absence of *VAMP2*. Mock, isotype control for each primary antibody. UI, uninfected.